Available online at www.sciencedirect.com
ScienceDirect
Nuclear Physics B 763 [FS] (2007) 309–329
NUCLEAR PHYSICS B

Dilute and collapsed phases of the self-gravitating gas

C. Destri [a,b], H.J. de Vega [c,d,*]

[a] *Dipartimento di Fisica G. Occhialini, Università Milano-Bicocca Piazza della Scienza 3, 20126 Milano, Italy*
[b] *INFN, Sezione di Milano, via Celoria 16, Milano, Italy*
[c] *LPTHE, Université Pierre et Marie Curie, Paris VI et Denis Diderot, Paris VII, Laboratoire Associé au CNRS UMR 7589, Tour 24, 5ème. étage, 4, Place Jussieu, 75252 Paris, Cedex 05, France*
[d] *Observatoire de Paris, LERMA, Laboratoire Associé au CNRS UMR 8112, 61, Avenue de l'Observatoire, 75014 Paris, France*

Received 18 May 2006; received in revised form 22 September 2006; accepted 31 October 2006

Available online 27 November 2006

Abstract

The self-gravitating gas in thermal equilibrium is studied using a Newtonian potential regularized at short distances. This short distance cutoff permits us to obtain a complete description of the gas including its collapsed phase. We give a field theory description of the N-body regularized self-gravitating gas in the canonical ensemble. The corresponding functional integral is dominated in the $N \to \infty$ limit by saddle points which provide a mean field description. The well-known dilute solutions (isothermal spheres) are recovered. We find new solutions which are regular in the regularized theory but become singular in the zero cutoff limit. They describe collapsed configurations where the particles are densely concentrated in a region of the size of the cutoff. These collapsed solutions provide the absolute minimum of the free energy. We find further new solutions which interpolate between the collapsed and the dilute configurations and describe tunneling processes where the gas collapses. The transition probability for such collapse processes turns out to be extremely small for large N. That is, the dilute solutions are in practice stable in the regime where they are locally stable.

1. Introduction

Selfgravitating system are ubiquitous in the universe. Selfgravity governs the formation and evolution of the large scale structure in the universe as well as the dynamics of galaxy formation,

* Corresponding author.
E-mail addresses: claudio.destri@mib.infn.it (C. Destri), devega@lpthe.jussieu.fr (H.J. de Vega).

0550-3213/$ – see front matter
doi:10.1016/j.nuclphysb.2006.10.028

stars and interstellar medium [1,2]. It is therefore of great interest to study self-gravitating fluids in thermal equilibrium although most astrophysical and cosmological systems are not in exact thermal equilibrium [1–8].

The self-gravitating gas has peculiar properties from the point of view of equilibrium statistical mechanics: The most important configurations are inhomogeneous and the thermodynamic functions *exist* in the *dilute* limit [5–7]

$$N \to \infty, \qquad V \to \infty, \qquad \frac{N}{V^{1/3}} \text{ fixed}, \tag{1.1}$$

where N is the number of particles and V stands for the volume of the box containing them. In such a limit, the internal energy, the free energy and the entropy turns to be extensive. That is, they take the form of N times a function of intensive dimensionless variables. In the case of a spherical box of radius R (so that $V = 4\pi R^3/3$) there is only one such variable, that is the ratio of the characteristic gravitational energy Gm^2N/R (m is the particle mass and G is Newton's constant) and the kinetic energy of the order of the temperature T of a particle in the gas [5–7]:

$$\eta = \frac{Gm^2N}{RT}.$$

For more complex geometries there will be, besides η (in such cases R is to be identified with the linear scale of the box), other dimensionless shape parameters.

In this paper we restrict the analysis to the simplest case of a spherical box and follow the approach of Refs. [5–7] where the starting point is the partition function for non-relativistic particles interacting through their gravitational attraction in thermal equilibrium. The configurational part of this partition function is expressed as a functional integral over a scalar field $\phi(\boldsymbol{x})$ [proportional to the gravitational potential] with an Euclidean action (that is minus the logarithm of statistical weight) proportional to N. Therefore, the saddle point technique (or mean field method) permits to compute the configuration partition function in the large N limit.

As investigated in Refs. [3,5–7] the self-gravitating gas in the canonical ensemble is in a gaseous phase for $0 \leqslant \eta < \eta_T$ where $\eta_T = 2.43450\ldots$. (Further studies on self-gravitating gases are reported in Refs. [4,8,9,11].) At this point the isothermal compressibility diverges and the speed of sound inside the sphere becomes imaginary. This clearly shows that the gas phase collapses at this point in the canonical ensemble as a consequence of the Jeans instability. Monte Carlo simulations explicitly show that the gas collapses for $\eta \gtrsim \eta_T$ into a very dense and compact phase [5].

It must be recalled that the small fluctuations around the mean field solution in the canonical ensemble are stable for $\eta < \eta_C = 2.517551\ldots$ [6]. Namely, fluctuations in the partition function do not feel the divergence of the isothermal compressibility neither the fact that the speed of sound becomes imaginary.

Even in the regime where the gaseous phase is locally stable there are always collapsed configurations which have much lower energy than the gas. In fact, the energy has its absolute minimum in the collapsed phase where all particles fall to one point and this configuration completely dominates the free energy, causing its divergence to minus infinity. Of course, interactions other than gravitational always dominate for short distances. Therefore, the properties the collapsed phase depend on the short distance physics. This physics is different according to the nature of the 'particles' considered. They can be from galaxies till molecules or atoms. Still, we can study the regime when collapse happens just introducing a short distance cutoff (ultraviolet regulator) to the gravitational interaction.

We present a complete description of the self-gravitating gas, including the collapsed phase, using a Newtonian potential regularized at short distances. We choose the Newton potential to be $-Gm^2/A$ for interparticle distances $r \leqslant A$ instead of Newton's law $-Gm^2/r$. The cutoff A is chosen very small compared with the size of the box.

We give an exact mapping of the N-body regularized problem into a field theory functional integral. This functional integral is dominated by its saddle points in the $N \to \infty$, namely by the mean field equations. The mean field equations coincide for zero cutoff with the Lane–Emden equation obtained from hydrostatics and assuming an ideal gas equation of state.

In this way we reproduce the well-known isothermal sphere solutions describing a self-gravitating gas in local thermal equilibrium. These diluted solutions get small corrections for small cutoff.

We find a host of new solutions (saddle points) from our regularized mean field equations. These new solutions are singular in the limit of zero cutoff and cannot be find from the standard (no cutoff) Lane–Emden equation. In these new solutions, which are perfectly regular for non-zero cutoff, a large number of particles concentrate near the origin. There are two new types of solutions.

The first type are the collapsed saddle point solutions: All the particles are densely concentrated in a region of size of the order of the cutoff. These solutions are studied analytically and provide the absolute minima of the free energy, which reads, at dominant order for small cutoff $A \ll R$:

$$F - F_0 \simeq -\frac{Gm^2 N(N-1)}{2A} + NT \log \frac{R^3}{(A/2)^3}.$$

Here, T is the temperature and F_0 is the free energy of an ideal gas. The first term is just the potential energy of N particles clustered in a small sphere of radius $A/2$, where the regularized gravitational interaction is the same for all $\frac{1}{2}N(N-1)$ particle pairs. The second term is T times the entropy loss in the collapse. This free energy is large and negative, unbounded from below as $A \to 0$. In particular, this free energy is well below the free energy of the dilute solution.

The second type of saddle point solutions interpolate between the gas phase and the collapsed phase, in a sort of pre-collapse. This solution has a finite action in the zero cutoff limit and describes the tunneling transition where a small fraction of particles coalesce into a region of the size of the short-distance regulator so that the density near the origin is very large. The tunneling probability to collapse for a dilute solution turns out to be extremely small for large N and small A. This means in practice that dilute solutions which are locally stable can be considered stable. As mentioned above this happens in the canonical ensemble for $0 \leqslant \eta < \eta_T$ where $\eta_T = 2.43450\ldots$.

The parameter η for the collapsed solutions can be arbitrarily large. That is, the particle density does not need to be dilute $N \sim V^{\frac{1}{3}}$ [see Eq. (1.1)] but we can have $N \sim V$.

We obtain in Section 5.2 an estimate for the lifetime for the dilute phase of the self-gravitating gas:

$$\tau \sim \frac{1}{a}\sqrt{\log\frac{1}{a}}\, e^{\frac{9N}{2\eta}a(\log a)^2} \sim \frac{R}{A}\sqrt{\log\frac{R}{A}}\exp\left[\frac{9AT}{2Gm^2}\left(\log\frac{R}{A}\right)^2\right].$$

One can see that the lifetime becomes infinitely long in the zero cutoff limit as well as when $N \to \infty$ at fixed cutoff [recall that $R \sim N$ in the dilute limit of Eq. (1.1)].

In summary, we provide through mean field theory a complete statistical description of the self-gravitating gas including the absolute minimum of the free energy.

2. Mean field approach to the self-gravitating gas

At short distances, the particle interaction for the self-gravitating gas in physical situations is not gravitational. Its exact nature depends on the problem under consideration (opacity limit, Van der Waals forces for molecules, etc.). We shall just assume a null short-distance pair force; that is, we consider the Hamiltonian

$$H_N = \sum_{j=1}^{N} \frac{p_j^2}{2m} - \sum_{j<k} \frac{Gm^2}{|\boldsymbol{q}_j - \boldsymbol{q}_k|_A},$$

where

$$|\boldsymbol{q}|_A = \begin{cases} |\boldsymbol{q}|, & \text{for } |\boldsymbol{q}| \geqslant A, \\ A, & \text{for } |\boldsymbol{q}| \leqslant A, \end{cases} \tag{2.1}$$

and $A \ll R$ is the short-distance cut-off.

It must be stressed that the results presented in this work using the soft-core cut-off Eq. (2.1) will be qualitatively the same for other types of cut-off since $R \gg A$.

The partition function in the canonical ensemble reads

$$Z_N = \frac{1}{N!\hbar^{3N}} \int \frac{d^{3N}p}{(2\pi)^{3N}} \int_{V^N} d^{3N}q\, e^{-\beta H_N}, \tag{2.2}$$

where $T \equiv \beta^{-1}$ is the temperature. Computing the integrals over the momenta $\boldsymbol{p}_j$ $(1 \leqslant j \leqslant N)$,

$$\int_{-\infty}^{+\infty} \frac{d^3p}{(2\pi)^3} \exp\left[-\frac{\beta p^2}{2m}\right] = \left(\frac{m}{2\pi\beta}\right)^{3/2},$$

yields

$$Z_N = Z_N^{(0)} Z_N^{\text{conf}}, \quad Z_N^{\text{conf}} = \frac{1}{V^N} \int_{V^N} d^{3N}q \prod_{1\leqslant j<k\leqslant N} \exp\left(\frac{Gm^2\beta}{|\boldsymbol{q}_j - \boldsymbol{q}_k|_A}\right), \tag{2.3}$$

where

$$Z_N^{(0)} = \left(\frac{2\pi m}{\beta\hbar^2}\right)^{3N/2} \frac{V^N}{N!} \equiv \exp\left[-\beta F^{(0)}\right]$$

is the partition function of the ideal gas. Thus,

$$F = F^{(0)} - T \log Z_N^{\text{conf}}$$

is the full canonical free energy.

We can now replace the integration over the particle coordinates with a functional integration over the configurations of the gravitational field φ produced by the particles. We start from the fundamental property of Gaussian functional integrals, namely

$$\int \mathcal{D}\varphi \exp\left\{-S[\varphi] + \int d^3x\, J(\boldsymbol{x})\varphi(\boldsymbol{x})\right\} = \exp\left[\frac{1}{2}\int d^3x \int d^3x'\, J(\boldsymbol{x})\mathcal{G}(\boldsymbol{x},\boldsymbol{x}')J(\boldsymbol{x}')\right], \tag{2.4}$$

where $S[\varphi]$ is the quadratic action functional

$$S[\varphi] = \frac{1}{2}\int d^3x \int d^3x'\, \varphi(\boldsymbol{x})\mathcal{G}^{-1}(\boldsymbol{x},\boldsymbol{x}')\varphi(\boldsymbol{x}')$$

and the integration measure is assumed to be normalized such that $\int \mathcal{D}\varphi \exp\{-S[\varphi]\} = 1$. Then we set

$$\mathcal{G}(\boldsymbol{x},\boldsymbol{x}') = \frac{G\beta^{-1}}{|\boldsymbol{x}-\boldsymbol{x}'|_A} \tag{2.5}$$

and we identify the source field $J(\boldsymbol{x})$ as βm times the microscopic particle density

$$J(\boldsymbol{x}) = \beta m \sum_{j=1}^{N} \delta^{(3)}(\boldsymbol{x}-\boldsymbol{q}_j). \tag{2.6}$$

Inserting Eqs. (2.5) and (2.6) into Eq. (2.4) yields,

$$\begin{aligned}\int \mathcal{D}\varphi \exp\left\{-S[\varphi] + \beta m \sum_{j=1}^{N}\varphi(\boldsymbol{q}_j)\right\} &= \exp\left[\frac{1}{2}\sum_{j,k=1}^{N}\frac{Gm^2\beta}{|\boldsymbol{q}_j-\boldsymbol{q}_k|_A}\right] \\ &= e^{\frac{Gm^2\beta N}{2A}} \prod_{1\leqslant j<k\leqslant N} \exp\left(\frac{Gm^2\beta}{|\boldsymbol{q}_j-\boldsymbol{q}_k|_A}\right).\end{aligned} \tag{2.7}$$

This provides a functional integral representation of the product over particle pairs in the integrand of Eq. (2.3). Inserting the identity Eq. (2.7) in Eq. (2.3) and exchanging the functional integration with the integration over the coordinates $\boldsymbol{q}_j$ we obtain

$$Z_N^{\text{conf}} = e^{-\frac{Gm^2\beta N}{2A}} \int D\varphi \exp\{-S[\varphi]\} \frac{1}{V^N} \int_{V^N} d^{3N}q \exp\left[\beta m \sum_{j=1}^{N}\varphi(\boldsymbol{q}_j)\right], \tag{2.8}$$

where

$$S[\varphi] = -\frac{\beta}{8\pi G}\int d^3x\, \varphi\nabla_A^2\varphi$$

and $\nabla_A^2 = -(4\pi G/\beta)\mathcal{G}^{-1}$ satisfies

$$-\nabla_A^2 \frac{1}{|\boldsymbol{x}-\boldsymbol{x}'|_A} = 4\pi\delta^{(3)}(\boldsymbol{x}-\boldsymbol{x}').$$

Since the $\boldsymbol{q}_j$ are dummy variables, we have

$$\int_{V^N} d^{3N}q \exp\left[\beta m \sum_{l=1}^{N}\varphi(\boldsymbol{q}_l)\right] = \left[\int_V d^3q\, e^{\beta m\varphi(\boldsymbol{q})}\right]^N$$

and the configuration partition function becomes

$$Z_N^{\text{conf}} = e^{-\frac{Gm^2\beta N}{2A}} \int \mathcal{D}\varphi\, e^{-S_{\text{eff}}[\varphi]}, \tag{2.9}$$

where

$$S_{\rm eff}[\varphi] = S[\varphi] + S_{\rm int}[\varphi], \quad S_{\rm int}[\varphi] \equiv -N \log\left[\frac{1}{V}\int\limits_V d^3x\, e^{-\beta m\varphi(\boldsymbol{x})}\right]. \tag{2.10}$$

We want to stress that this field-theoretic functional formulation of the self-gravitating gas is fully equivalent, for any N, to the original one in terms of particles. The functional integral representation of the partition function presented in Refs. [5,6] for the canonical ensemble is slightly different but equivalent to Eqs. (2.9) and (2.10) for large N. Let us also observe that the nonlocal operator ∇_A^2 reduces to the standard Laplacian operator in the limit $A \to 0$. However, this limit is not so straightforward in the functional integral above, since the interaction term $S_{\rm int}$ in the action may (and indeed does) become unbounded from below in such limit.

We now pass to dimensionless variables by setting $\boldsymbol{r} = \boldsymbol{x}/R$ and

$$-\beta m\varphi(\boldsymbol{x}) = \phi(\boldsymbol{r})$$

The action for $\phi(\boldsymbol{x})$ now reads

$$S_{\rm eff}[\varphi] = N s[\phi], \quad s[\phi] = -\frac{1}{8\pi\eta}\int d^3r\, \phi\nabla_a^2\phi - \log\left[\int\limits_{|\boldsymbol{r}|\leqslant 1} d^3r\, e^{\phi}\right] + \log\frac{4\pi}{3}, \tag{2.11}$$

where

$$\eta \equiv \frac{Gm^2\beta N}{R}, \qquad a \equiv \frac{A}{R}, \qquad -\nabla_a^2\frac{1}{|\boldsymbol{r}-\boldsymbol{r}'|_a} = 4\pi\delta^{(3)}(\boldsymbol{r}-\boldsymbol{r}'). \tag{2.12}$$

We recall that the variable η is the ratio of the characteristic gravitational energy $\frac{Gm^2N}{R}$ and the kinetic energy $\sim T = \beta^{-1}$ of a particle in the gas. For $\eta = 0$ the ideal gas is recovered.

Having factored out of the action the number of particles N, it is natural to use the saddle points method to evaluate the functional integral over ϕ in the limit $N \to \infty$ at fixed η, that is in the dilute limit. Strictly speaking, however, the action per particle $s[\phi]$ still depends on N through $a = A/R \propto A/N$. Thus we should better regard the saddle point method as a mean field type approximation yielding the free energy F to leading order in N, as we shall now show. The stationarity condition

$$\frac{\delta s[\phi]}{\delta\phi(\boldsymbol{r})} = 0$$

leads to the regularized self-consistent Boltzmann–Poisson equation

$$\nabla_a^2\phi + \frac{4\pi\eta}{Q}e^{\phi} = 0, \quad Q \equiv \int\limits_{|\boldsymbol{r}|\leqslant 1} d^3r\, e^{\phi(\boldsymbol{r})}, \quad \text{for } |\boldsymbol{r}| \leqslant 1, \quad \text{and}$$

$$\nabla_a^2\phi = 0, \quad \text{for } |\boldsymbol{r}| \geqslant 1. \tag{2.13}$$

In the limit $a \to 0$ this becomes the standard self-consistent Boltzmann–Poisson (or Lane–Emden) equation derivable from hydrostatic plus the assumption of a local, ideal gas equation of state [3].

We may rewrite Eq. (2.13) in integral form as

$$\phi(\boldsymbol{r}) = \eta\int d^3r'\frac{\rho(\boldsymbol{r}')}{|\boldsymbol{r}-\boldsymbol{r}'|_a}, \tag{2.14}$$

where

$$\rho(\boldsymbol{r}) = \frac{e^{\phi(\boldsymbol{r})}}{Q} \quad \text{for } |\boldsymbol{r}| \leqslant 1, \qquad \rho(\boldsymbol{r}) = 0 \quad \text{for } |\boldsymbol{r}| > 1, \quad \int d^3r\, \rho(\boldsymbol{r}) = 1, \tag{2.15}$$

is the normalized particle density associated to $\phi(\boldsymbol{r})$.

We may also use the identity involving the standard Laplacian ∇^2,

$$-\nabla^2 \frac{1}{|\boldsymbol{r} - \boldsymbol{r}'|_a} = \frac{1}{a^2}\delta\big(|\boldsymbol{r} - \boldsymbol{r}'| - a\big),$$

to cast the field equation in the integro-differential form

$$\nabla^2\phi(\boldsymbol{r}) = -\frac{\eta}{Qa^2} \int\limits_{|\boldsymbol{r}'|\leqslant 1} d^3R'\, \delta\big(|\boldsymbol{r} - \boldsymbol{r}'| - a\big) e^{\phi(\boldsymbol{r}')}. \tag{2.16}$$

Notice that the Laplacian in the origin is always regular for nonzero cutoff

$$\nabla^2\phi(0) = -\frac{\eta}{Qa^2} \int\limits_{|\boldsymbol{r}'|\leqslant 1} d^3r'\, \delta\big(|\boldsymbol{r}'| - a\big) e^{\phi(\boldsymbol{r}')}, \tag{2.17}$$

implying, together with the finiteness of $\phi(0)$, that $\nabla\phi = 0$ in the origin.

We can recast the action of the saddle point Eq. (2.11) using the regularized equation of motion (2.13) as follows,

$$s[\phi] = \frac{1}{2Q} \int\limits_{|\boldsymbol{r}|\leqslant 1} d^3r\, \phi(\boldsymbol{r}) e^{\phi(\boldsymbol{r})} - \log\frac{3Q}{4\pi}. \tag{2.18}$$

The free energy for large N can be written in terms of the stationary action as [5]

$$F = F_0 + N\frac{Gm^2}{2A} + NTs(\eta, a) + \mathcal{O}(1) \quad \text{(at fixed } a\text{)}, \tag{2.19}$$

where $s(\eta, a) \equiv s[\phi_s]$, ϕ_s is a solution of Eq. (2.13), and F_0 is the free energy for the ideal gas. Notice that, since a vanishes as N^{-1} as $N \to \infty$ *at fixed A and* η, we can regard $NTs(\eta, a)$ as extensive in the particle number, that is linear in N, only if it is regular as $a \to 0$. This holds true for stationary point which are regular at the $a = 0$ limit. We show below that there are saddle points which become singular in the $a \to 0$ limit and consequently the free energy is not proportional to N. Similarly, the subleading terms in Eq. (2.19) are order one only for saddle points which are regular for $a = 0$. What is always true is that they are indeed subleading for any given saddle point.

3. Spherically symmetric solutions

In the case of spherically symmetry the integration over angles in Eq. (2.16) can be performed explicitly, yielding the one-dimensional non-linear integro-differential equation

$$\frac{\partial^2}{\partial r^2}\big[r\phi(r)\big] = -\frac{2\pi\eta}{Qa} \int\limits_{|r-a|}^{r+a} dr'\, r' e^{\phi(r')}, \tag{3.1}$$

where now

$$Q = 4\pi \int_0^1 dr\, r^2 e^{\phi(r)}. \tag{3.2}$$

Eq. (3.1) is to be supplemented with the boundary conditions of smooth joining (continuity of $\phi(r)$ and $\phi'(r)$ at $r = 1 + a$) with the external monopole solution $\phi(r) = \eta/r$.

Integration over the angles in Eq. (2.14) yields the non-linear integral equation

$$\phi(r) = \frac{4\pi\eta}{Q}\left\{ \frac{1}{\max(r,a)} \int_0^{|r-a|} dr'\, r'^2 e^{\phi(r')} + \theta(1-r-a) \int_{r+a}^1 dr'\, r' e^{\phi(r')} \right.$$
$$\left. - \frac{1}{2r} \int_{|r-a|}^{r+a} dr'\, r' \left[\frac{a}{2} - r - r' - \frac{(r-r')^2}{2a} \right] e^{\phi(r')} \theta(1-r') \right\}, \tag{3.3}$$

which by itself determines $\phi(r)$ for all values of r. In particular Eq. (3.3) implies that any solution is finite in the origin, since

$$\phi(0) = \frac{4\pi\eta}{Q}\left[\frac{1}{a} \int_0^a dr\, r^2 e^{\phi(r)} + \int_a^1 dr\, r e^{\phi(r)} \right]. \tag{3.4}$$

Moreover, Eq. (3.1) or Eq. (3.3) imply

$$\phi'(0) = 0 \quad \text{and} \quad \phi'(r) < 0 \quad \text{for } r > 0, \tag{3.5}$$

so that the density is monotonically decreasing away from the origin. The simplest way to prove that $\phi'(0) \leqslant 0$ is to multiply both sides of Eq. (3.1) by r and integrate from 0 to an arbitrary value. This yields

$$\phi'(r) = -\frac{2\pi\eta}{Qar^2} \int_0^r dr'\, r' \int_{|r'-a|}^{r'+a} dr''\, r'' e^{\phi(r'')},$$

which has a negative definite r.h.s. which vanishes when $r \to 0$ as long as $a > 0$.

The action for spherically symmetric solution becomes from Eq. (2.18),

$$s[\phi] = \frac{2\pi}{Q} \int_0^1 r^2\, dr\, \phi(r) e^{\phi(r)} - \log \frac{3Q}{4\pi}. \tag{3.6}$$

4. Solutions regular as $A \to 0$

The saddle point equation (2.13) admits solutions which are regular as $a \to 0$ and reproduce in this limit the solutions of the standard Lane–Emden equation. We call them dilute solutions. These are known since longtime in the spherically symmetric case [3]. To study such solutions we can set the cutoff A to zero from the start. Equivalently, one can take the limit $a \to 0$ in Eq. (3.1) with the assumption that $\phi(r)$ stays finite in the limit for any r, including the origin $r = 0$, and that $\phi'(0) = 0$.

Assuming spherical symmetry we get $\phi(r) = \eta/r$ for $r \geqslant 1$, while for $r \leqslant 1$ we have

$$\phi''(r) + \frac{2}{r}\phi'(r) + \frac{4\pi\eta}{Q}e^{\phi(r)} = 0, \quad \phi'(0) = 0, \tag{4.1}$$

with the boundary conditions

$$\phi(1) = \eta, \qquad \phi'(1) = -\eta. \tag{4.2}$$

Clearly there exists one and only one solution for a given Q, so the classification of all solutions is equivalent to the determination of all the allowed values of Q.

We set as usual [5]

$$\phi(r) = \phi(0) + \chi(\lambda r), \quad \phi(0) = \log\frac{Q\lambda^2}{4\pi\eta}, \quad \chi(0) = 0, \tag{4.3}$$

where $\chi(z)$ must satisfy, upon inserting Eq. (4.3) in Eq. (4.1),

$$\chi''(z) + \frac{2}{z}\chi'(z) + e^{\chi(z)} = 0, \quad \chi'(0) = 0 \tag{4.4}$$

and, from the boundary conditions Eq. (4.2) at $r = 1$,

$$\log\frac{Q\lambda^2}{4\pi\eta} + \chi(\lambda) = \eta, \qquad \lambda\chi'(\lambda) = -\eta. \tag{4.5}$$

These two relations fix the two parameters Q and λ as functions of η. In particular, we can rewrite $\phi(r)$ as

$$\phi(r;\eta) = \eta - \chi\big(\lambda(\eta)\big) + \chi\big(\lambda(\eta)r\big). \tag{4.6}$$

The density profile of Eq. (2.15) reads in terms of $\chi(\lambda r)$,

$$\rho(r) = \frac{\lambda^2}{4\pi\eta}e^{\chi(\lambda r)}, \tag{4.7}$$

so that the normalization factor can also be written $Q = e^{\eta}/\rho(1)$.

Due to scale-invariant behaviour of the gravitational interaction, Eq. (4.4) enjoys the following scale covariance property: If $\chi(z)$ is a solution, then also $\chi_\alpha(z) \equiv \chi(ze^{\alpha}) + 2\alpha$ is a solution. Using $\chi_\alpha(z)$ rather than $\chi(z)$ is compensated by the shift $\lambda \to \lambda e^{-\alpha}$. Notice that $\phi(r)$ is indeed defined as a scale transformation of $\chi(z)$, with the scale parameter λ (not uniquely) fixed by $\lambda\chi'(\lambda) = -\eta$. As a consequence of this scale invariance all physical quantities must be invariant under the simultaneous replacements $\lambda \to \lambda e^{-\alpha}$ and $\chi(\lambda) \to \chi(\lambda) + 2\alpha$.

Let us observe that, if the solutions of Eq. (4.1) or (4.4) did not fulfill $\phi'(0) = 0$ or $\chi'(0) = 0$, a delta function at the origin would appear in the right-hand side and $\chi(z) \simeq -A/z$, with $A > 0$, when $z \to 0$. This is the only possible singular behaviour and corresponds to a point particle with negative mass $-A$ in the origin. We shall not consider such unphysical solutions, which are ruled out when Eq. (4.1) is considered as the $a \to 0$ limit of Eq. (3.1), and stick to $\chi'(0) = 0$.

Moreover, scale invariance allows to set also $\chi(0) = 0$. This choice completely fixes the scale and we have no more scale invariance left. One has from the second Eq. (4.5) that $\chi'(z) < 0$ for all positive z, so that the density profile is monotonically decreasing with the distance.

Since $\chi(z)$ is monotonically decreasing, the allowed values of Q [that is of $\rho(1)$, see Eqs. (2.15) and (4.2)] are in one-to-one correspondence with to the roots of the relation $\lambda = \lambda(\eta)$ which inverts the second of Eqs. (4.5). Thus there is only one dilute solution for each value

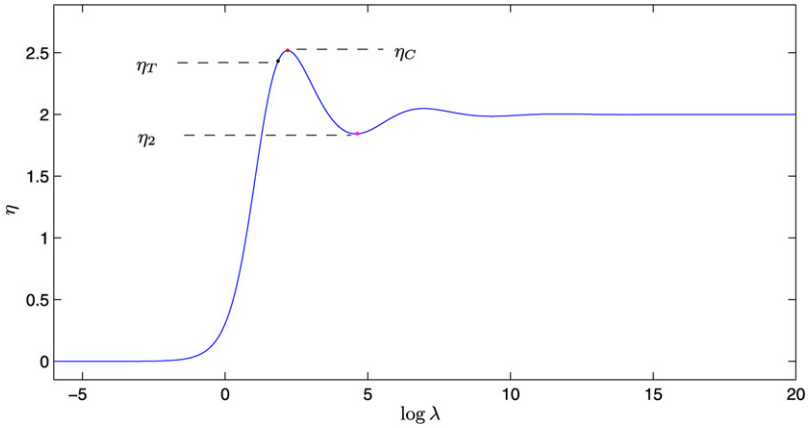

Fig. 1. η as a function of $\log\lambda$ according to Eq. (4.5) for the dilute solutions. Notice the maximum of η at $\eta_C = 2.51755\ldots$, where c_V diverges. The region beyond the maximum location, at $\log\lambda_C = 2.196459\ldots$, is locally unstable as discussed in Ref. [6]. c_P and κ_T diverge before the maximum, at the point $\eta_T = 2.43450\ldots$.

of λ. However, $\lambda = \lambda(\eta)$ is a multiple valued function for a certain range of η. We plot η vs. $\log\lambda$ in Fig. 1. One sees that there is a unique λ for a given η only for $\lambda < 3.6358865\ldots$, that is $\eta < \eta_2 \equiv 1.84273139\ldots$. For $\eta_2 < \eta < \eta_C \equiv 2.517551\ldots$ (η_C is the absolute maximum, located at $\lambda_C = 8.99311\ldots$, of $-\lambda\chi'(\lambda)$ over $0 < \lambda < \infty$) the relation $\lambda = \lambda(\eta)$ is indeed multivalued and as η approches the value 2 there are increasingly more solutions which accumulate near the purely logarithmic solution

$$\phi_\infty(r) = \lim_{\lambda\to\infty}\big[\eta - \chi(\lambda) + \chi(\lambda r)\big] = 2 - 2\log r,$$

which correspond to the singular density profile $\rho_\infty(r) = (4\pi r^2)^{-1}$. In other words, when η is exactly 2 there exist an infinite set of solutions corresponding to the increasing sequence of values of λ which satisfy $\lambda\chi'(\lambda) = -2$. In Fig. 2 we plot in log–log scale the density profile $\rho(r)$ [see Eq. (4.7)] vs. r for few terms of this sequence.

We recall that, for any given $\eta < \eta_C$, only the unique dilute solution with $\lambda < \lambda_C$ is locally stable. That is, any small fluctuation increases the action. At $\lambda = \lambda_C$ a zero-mode appears in the linear fluctuation spectrum and c_V, the specific heat at constant volume, diverges. For larger values of λ negative modes show up, signalling local instability. Actually the locally stable dilute solutions describe a (locally) stable dilute phase, in the thermodynamic and mechanical terms, only for $\eta < \eta_T = 2.43450\ldots$. At $\lambda = \lambda_T = 6.45071\ldots$ the isothermal compressibility diverges and the speed of sound inside the sphere becomes imaginary. The gas phase collapses at this point in the canonical ensemble as a consequence of the Jeans instability. This is confirmed by Monte Carlo simulations [5]. Hence, in the case $\eta = 2$ depicted in Fig. 2, only the solution with the smallest density contrast, corresponding to the smallest value $\lambda = 4.071496\ldots$, is stable. The unstable solutions that exist for $\eta_2 < \eta < \eta_T$ should imply that the dilute phase is metastable for this range of η, However, their lifetime is so huge [see Eq. (5.20)] that these dilute solutions are in practice stable.

In the stable dilute phase the particles are moderately clustered around the origin with a density that monotonically decreases with r. One sees that the density contrast between the center

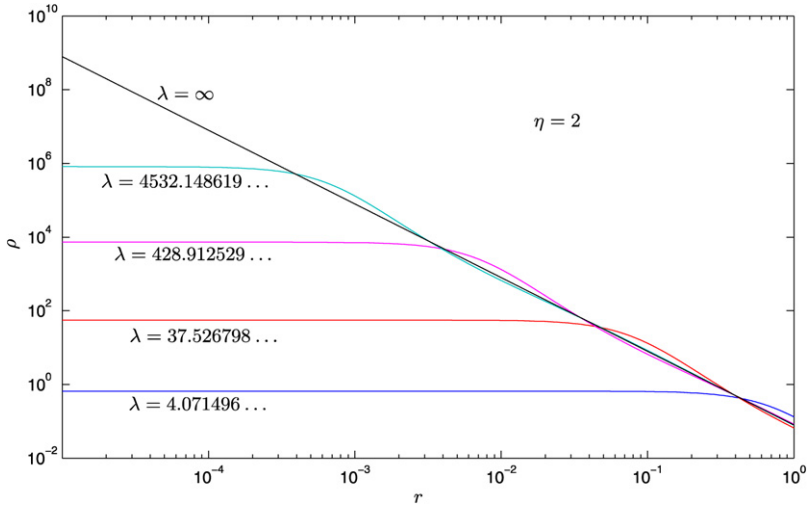

Fig. 2. Log–log plot of the density profile for some dilute solutions at $\eta = 2$. Only the smallest one at $\lambda = 4.071496\ldots$ is locally stable.

and the boundary

$$\frac{\rho(0)}{\rho(1)} = e^{-\chi(\lambda)}$$

grows with λ since $\chi(\lambda)$ decreases with λ [see Eq. (4.5)] and Fig. 2 [3,5,6].

The action per particle of a dilute solution can be written entirely in terms of the density at the border [5]

$$s(\eta) = 3 - \eta + \log\left[\frac{4\pi}{3}\rho(1)\right] - 4\pi\rho(1) = 3 - \eta + \log\frac{\lambda^2}{3\eta} + \chi(\lambda) - \frac{\lambda^2}{\eta}e^{\chi(\lambda)}, \tag{4.8}$$

and is multivalued for $\eta_2 \ldots < \eta < \eta_C \ldots$. The solution with the smallest density contrast has the smallest action, in accordance with the linear stability analysis. We plot $s(\eta)$ as a function of $\log\lambda$ and η in Fig. 3.

All physical quantities can be expressed for large N in terms of the function

$$f(\eta) \equiv 1 + \frac{\eta}{3}\frac{ds}{d\eta} = \frac{4\pi}{3}\rho(1). \tag{4.9}$$

We have for the energy, the pressure, the isothermal compressibility κ_T, the specific heats (c_V and c_P) and the speed of sound at the boundary [5]

$$\frac{E}{3NT} = f(\eta) - \frac{1}{2} + \mathcal{O}\left(\frac{1}{N}\right), \qquad \frac{pV}{NT} = f(\eta) + \mathcal{O}\left(\frac{1}{N}\right),$$
$$\frac{S - S_0}{N} = -3\big[1 - f(\eta)\big] - s(\eta) + \mathcal{O}\left(\frac{1}{N}\right), \qquad \kappa_T = \frac{1}{f(\eta) + \frac{1}{3}\eta f'(\eta)} + \mathcal{O}\left(\frac{1}{N}\right),$$
$$c_V = 3\left[f(\eta) - \eta f'(\eta) - \frac{1}{2}\right] + \mathcal{O}\left(\frac{1}{N}\right), \qquad c_P = c_V + \frac{[f(\eta) - \eta f'(\eta)]^2}{f(\eta) + \frac{1}{3}\eta f'(\eta)} + \mathcal{O}\left(\frac{1}{N}\right),$$

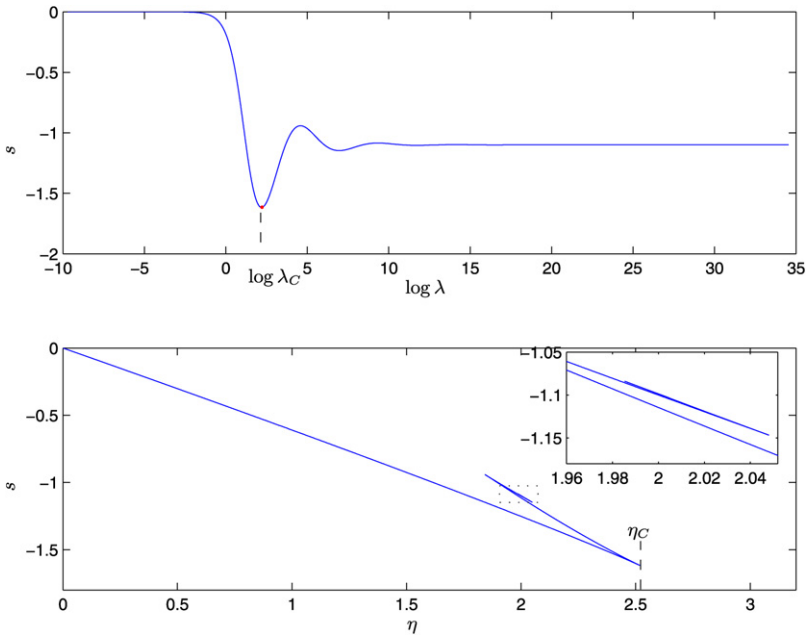

Fig. 3. The action per particle s vs. $\log\lambda$ (above) and vs. η (below) for the dilute solution. $s(\eta)$ is multivalued for $\eta > \eta_2$, with a peculiar self-similar structure, as evident from the inset.

$$\frac{v_s^2}{T} = \frac{[f(\eta) - \eta f'(\eta)]^2}{3\left[f(\eta) - \eta f'(\eta) - \frac{1}{2}\right]} + f(\eta) + \frac{1}{3}\eta f'(\eta) + \mathcal{O}\left(\frac{1}{N}\right). \tag{4.10}$$

Here S_0 stands for the entropy of the ideal gas.

Notice that κ_T and c_P, the specific heat at constant pressure, both diverge before η_C, at $\eta = \eta_T \equiv 2.43450\ldots$ [5]. Moreover, the speed of sound squared, which stays regular at the boundary when $\eta \to \eta_T$, has a simple pole there when evaluated inside the isothermal sphere [5]. Thus, when $\eta > \eta_T$ the speed of sound is purely imaginary inside the sphere implying that small fluctuations grow exponentially with time.

We have here discussed the dilute solutions in the zero cutoff limit ($A = 0$). Including the short distance cutoff only adds small $\mathcal{O}(A)$ corrections to the dilute solutions.

5. Solutions singular as $A \to 0$

We present in this section new solutions for which the mean field $\phi(r)$ develops singularities in the limit $A \to 0$. In case of spherical symmetry, when Eq. (3.1) is the saddle point equation, the only possible singularity is localized at $r = 0$. It is convenient then to 'blow up' the region near $r = 0$ by setting [compare with Eq. (4.3)]

$$\phi(r) = \phi(0) + \mu^2 \xi\left(\frac{r}{a}\right), \quad \phi(0) = \log\frac{Q\lambda^2}{4\pi\eta}, \quad \xi(0) = 0, \quad \text{so that } \rho(r) = \frac{\lambda^2}{4\pi\eta} e^{\mu^2\xi\left(\frac{r}{a}\right)}, \tag{5.1}$$

where we introduce the variable:

$$\mu \equiv \lambda a.$$

We thus obtain for $\xi(x)$, $x = r/a$, the following rewriting of the integral equation (3.3)

$$\begin{aligned}\xi(x) = {} & \frac{1}{\max(x,1)} I_2\big(|x-1|\big) - I_1\big(m(x)\big) - \frac{(x-1)^2}{4x}\big[I_1\big(m(x)\big) - I_1\big(|x-1|\big)\big] \\ & + \frac{x+1}{2x}\big[I_2\big(m(x)\big) - I_2\big(|x-1|\big)\big] - \frac{1}{4x}\big[I_3\big(m(x)\big) - I_3\big(|x-1|\big)\big] \\ & - I_2(1) + I_1(1),\end{aligned} \tag{5.2}$$

where,

$$m(x) \equiv \min\left(\frac{1}{a}, x+1\right), \qquad I_n(x) \equiv \int_0^x dy\, y^n \exp\big[\mu^2 \xi(y)\big], \tag{5.3}$$

and we have used Eq. (3.4) to write $\phi(0)$ in terms of $\xi(x)$ as

$$\phi(0) = \mu^2\left[I_2(1) + I_1\left(\frac{1}{a}\right) - I_1(1)\right]. \tag{5.4}$$

Notice that all dependence on λ appears now through the variable $\mu = \lambda a$.

By construction we have $\xi'(0) = 0$ [see Eq. (3.5)], $\xi(0) = 0$ and $\xi'(x) < 0, \xi(x) < 0$ for all $x > 0$. Notice that η does not enter the integral equation above, just as it did not enter the differential equation (4.4) for χ in the setup without short-distance regulator. Owing to the normalization condition Eq. (3.2), η is *computed* once a solution is known, as a function of μ (and a), through

$$\eta = \mu^2 a I_2\left(\frac{1}{a}\right) = \mu^2 a \int_0^{\frac{1}{a}} dx\, x^2 \exp\big[\mu^2 \xi(x)\big]. \tag{5.5}$$

From Eq. (3.1) we may also derive the integro-differential form of the equation satisfied by $\xi(x)$, that is

$$\frac{\partial^2}{\partial r^2}\big[x\xi(x)\big] = -\frac{1}{2}\big[I_1(x+1) - I_1\big(|x-1|\big)\big]. \tag{5.6}$$

Eq. (5.2) or (5.6) can be solved numerically to high accuracy for any given μ. We plot the corresponding η as a function of $\log\lambda$ in Fig. 4, for better comparison with its behaviour in the dilute case, Fig. 1.

We find *four* different regimes according to the value of μ for $a \ll 1$.

- $\mu = \mathcal{O}(a)$. That is, $\lambda = \mathcal{O}(1)$. In this regime we reproduce the curve $\eta = \eta(\lambda)$ (Fig. 1) characteristic of the diluted phase of Section 4 plus small corrections of order a.
- $\mu = \mathcal{O}(1)$. Here $\lambda = \mathcal{O}(\frac{1}{a})$ and the damped oscillation pattern around $\eta = 2$, characteristic of the dilute solutions, gets disrupted: The oscillations regain larger and larger amplitude until $\mu^2 = \lambda^2 a^2 \sim \log\frac{1}{a}$.
- $\mu^2 = \mathcal{O}(\log\frac{1}{a})$. Here, a sudden drop to very small $\eta = \eta_{\min}(a) \sim a$ takes place [see Fig. 4]; then η rises again as μa, for μa large enough, and keep growing indefinitely (see Fig. 4 and below). This regime corresponds to saddles interpolating between the dilute phase and a collapsed phase (see below).
- $\mu^2 = \mathcal{O}(\frac{1}{a})$. This regime describes collapsed configurations where all particles are concentrated in a region of size $\sim a$ and provide the absolute minimum of the free energy.

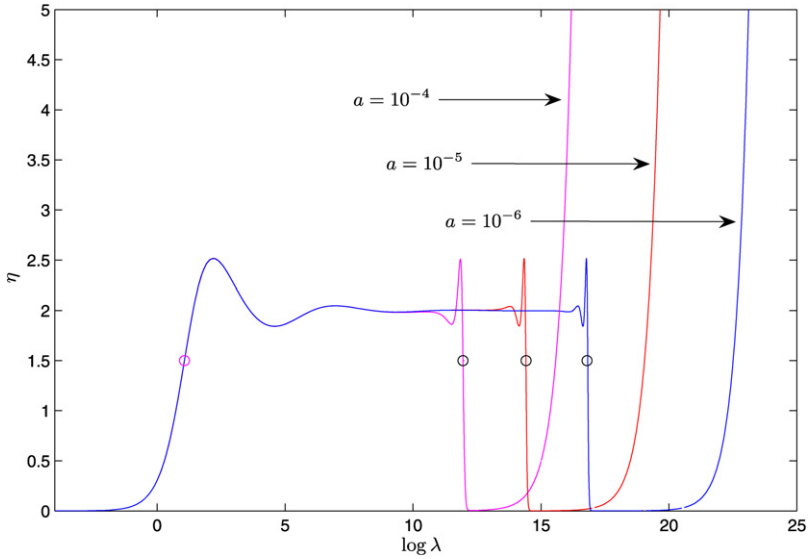

Fig. 4. η as a function of $\log\lambda$ according to Eq. (5.5). The black circle mark the values of λ corresponding to the interpolating solutions depicted in Fig. 5. Here, $\mu^2 \equiv \lambda^2 a^2 = \mathcal{O}(\log \frac{1}{a})$.

Notice that new maxima appear in addition to those present for $a = 0$ (compare with Fig. 1). Those new maxima turn to be degenerate with the old ones up to small corrections of order a. In addition, η exhibits oscillations for $\mu = \mathcal{O}(1)$ which are similar to those present at $a = 0$ and $\eta \to 2$ but reversed and faster. We shall give below a qualitative explanation for this peculiar behavior.

The new dependence of η on λ described above implies that the number of solutions (that is the number of distinct λ for any given η) is finite for any η and that, most importantly, there appear new solutions. In particular, there are two new solutions for $\eta_{\min}(a) < \eta < \eta_2$ in addition to the unique solution regular as $a \to 0$ and there is one new solution for $\eta > \eta_C$, the region not accessible to dilute solutions. These new solutions are singular in the limit $a \to 0$, as evident from Fig. 5, where we plot $\phi(r)$ vs. r for few values of a at a fixed value of η and λ placed in the sudden drop of η vs. $\log\lambda$ (the black circles in Fig. 4, scaling as $\mu^2 = \lambda^2 a^2 \sim \log \frac{1}{a}$).

In Fig. 5 we also compare the solutions of the integral equation (3.3) or (5.2) to those of the differential equation (4.1), with boundary conditions (4.2), in which Q takes the value obtained by the integral method, upon using Eqs. (5.1) and (5.4). We see that the agreement is very good down to r of order a, when the short-distance regularization becomes effective, while the solutions of the differential equation (4.1) eventually blow to $-\infty$ as $r \to 0$. This agreement appears very natural from the integro-differential formulation of Eq. (3.1), where the short-distance regulator a can play a significant role only for $r \lesssim a$.

Hence, the qualitative behaviour of the singular solutions can be understood already from the differential equation (4.4), provided one drops the initial conditions $\chi(0) = \chi'(0) = 0$ characteristic of the dilute solutions. That is, using the relation $\chi(\mu x) = \mu^2 \xi(x)$ that follows from Eqs. (4.3) and (5.1), we can solve the integral equation (5.2) just in the interval $0 \leqslant x \leqslant x_1$, with $x_1 \gtrsim 2$, to compute

$$\chi(2\mu) = \mu^2 \xi(x_1) \quad \text{and} \quad \chi'(2\mu) = \mu \xi'(x_1), \tag{5.7}$$

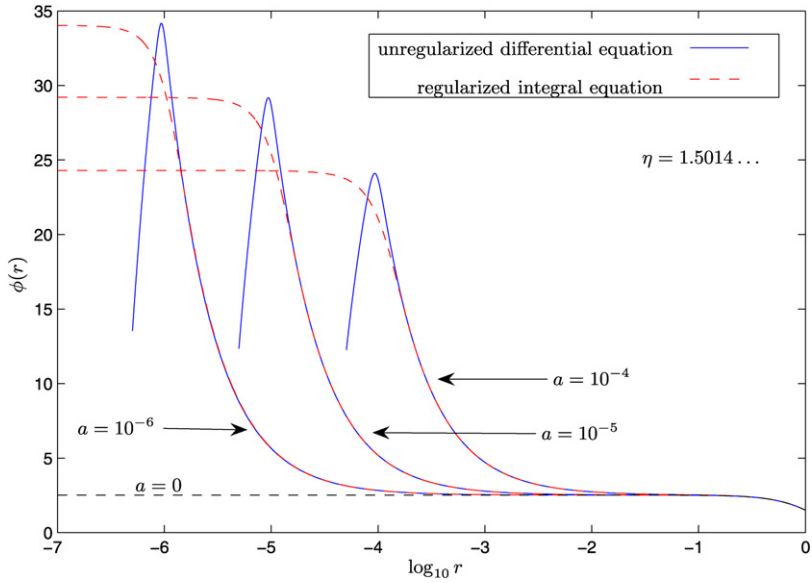

Fig. 5. Profiles of the mean field $\phi(r)$ for $\mu^2 = \mathcal{O}(\log \frac{1}{a})$ (interpolating solutions), with comparison between the regularized and unregularized cases. The dashed black curve is the dilute solution (that is for $a = 0$) at the same value of η, namely at the location of the magenta circle of Fig. 4. The other curves correspond to the black circles in Fig. 4.

at the boundary $x = x_1$. These values for $\chi(2\mu)$ and $\chi'(2\mu)$, both negative by construction, can then be used as initial conditions at $z = 2\mu$ to solve the differential equation (4.4) in place of the conditions $\chi(0) = \chi'(0) = 0$, characteristic of the dilute solutions. The choice $x_1 \gtrsim 2$ is motivated by a direct numerical analysis but can be explained by the fact that μ diverges when $a \to 0$ in the solutions which are singular as $a \to 0$. This implies, on one side, that the r.h.s. of Eq. (5.6) is exponentially small in μ^2 when $x_0 \gtrsim 2$ [see also Eq. (5.3)] and, on the other side, that the initial conditions at $z = 2\mu$ affect the function $\chi(z)$ very strongly, causing the rapid drop for $r > 2a$ observed in Fig. 5, as well as the growth followed by the fall to $-\infty$ as $r \to 0$. It must be observed, in fact, that $\xi(x)$ has a finite limit as $\mu \to \infty$ [see below Eq. (5.9)], so that to leading order and $\mu \gg 1$, using Eq. (5.7),

$$\chi(2\mu) = \mathcal{O}\big(\mu^2\big) \quad \text{and} \quad \chi'(2\mu) = \mathcal{O}(\mu).$$

It follows that the function $\chi(z)$ fulfills approximately the free equation $(z\chi)'' = 0$ in the rapid drop for $z > 2\mu$ as well as in the following plateau (to the right in Fig. 5), that is

$$\chi(z) \simeq \frac{c_0}{z} + c_1, \qquad c_0 = \mathcal{O}\big(\mu^3\big), \quad c_1 = \mathcal{O}\big(\mu^2\big). \tag{5.8}$$

Where we used that $z = \lambda r = \mu x$. This behaviour is valid as long as $\chi''(z) \lesssim e^{\chi(z)}$, that is $z \lesssim \mathcal{O}(\mu \exp[\mu^2/3])$ since $\chi = \mathcal{O}(\mu^2)$ and $c_0 = \mathcal{O}(\mu^3)$. For larger values of z the function $\chi(z)$ tends to the unique large distance fixed point given by the purely logarithmic solution $\log(2/z^2)$ and does this through the characteristic damped harmonic oscillations in $\log \lambda$ [3] responsible for the waving behaviour of η in the dilute phase [see Fig. 1]. Since the crossover to the logarithmic behaviour takes place for larger and larger values of z the smaller is a, because $\mu = \mathcal{O}(\sqrt{\log \frac{1}{a}})$ grows with a as well as the crossover point $z = \mathcal{O}(\mu \exp[\mu^2/3])$. When $\chi(z)$ is almost constant,

the characteristic oscillations tend to have the same amplitude they have in the regular solutions. Moreover, this almost constant value of $\chi(z)$, which is of order μ^2, decreases faster in μ than the end point $\lambda = \mu/a$ at which $\chi(z)$ is to be evaluated to give η as in the second of Eqs. (4.5). This explain why the oscillations of η are reversed and faster right before the sudden drop in Fig. 4. In other words, the oscillations in the left part of Fig. 4 describe the approach to the limiting solution $\log(2/z^2)$ [$\eta = 2$] while one is getting *off* this limiting solution in the right part of Fig. 4. This explains why the oscillations on the right get reversed compared with the oscillations on the left of Fig. 4.

In the next two subsections we will provide more details on all these matters and further analytical insights.

5.1. Collapsed phase

This is the case when $\mu \sim \eta/a$ as $a \to 0$ and corresponds to the growing branch on the right of Fig. 4. Notice that we have collapsed solutions for arbitrarily large values of η contrary to the dilute solutions which only exist for $\eta < \eta_C$.

Since $\xi(x)$ is negative and monotonically decreasing for $x > 0$, the quantity $\exp[\mu\xi(x)]$ is exponentially small except in the interval $0 \leqslant x < x_0$ where $\xi(x)$ would vanish in the limit. We use now this property to get an approximate but analytic singular solution. That is, the dominant contribution in the r.h.s. of Eq. (5.2) is obtained when all integrations are restricted to the interval $0 \leqslant x \leqslant x_0$. One easily realizes that, by consistency, $x_0 = 1/2$. Then one finds

$$I_n(x) = \frac{1}{n+1} \begin{cases} x^{n+1}, & x \leqslant 1/2, \\ 2^{-n-1}, & x \geqslant 1/2, \end{cases}$$

and in particular using Eqs. (5.4) and (5.5),

$$\phi(0) = \mu^2 \left[I_2(1) + I_1\left(\frac{1}{a}\right) - I_1(1) \right] = \frac{\mu^2}{24}, \qquad \eta = \mu^2 a I_2\left(\frac{1}{a}\right) = \frac{\mu^2 a}{24}, \qquad \phi(0) = \frac{\eta}{a}.$$

Finally, the leading form for $\phi(r)$ reads

$$\phi(r) = \phi(0) + \frac{24\eta}{a}\xi\left(\frac{r}{a}\right) = \begin{cases} \frac{\eta}{a}, & r \leqslant a/2, \\ \frac{\eta}{a} + \frac{\eta}{2r}\left(\frac{r}{a} - \frac{1}{2}\right)^3\left(\frac{r}{a} - \frac{5}{2}\right), & a/2 \leqslant r \leqslant 3a/2, \\ \frac{\eta}{r}, & r \geqslant 3a/2. \end{cases} \tag{5.9}$$

Notice that $\phi(r)$ as well as its first and second derivatives are continuous at $r = a/2$ and $r = 3a/2$. For $r \geqslant 3a/2$, the effective gravitational field has the free form proper of a locally vanishing mass density.

Higher corrections can be obtained by iteration over Eq. (5.2). That is, using the leading form of $\xi(x)$ that can be read out of in Eq. (5.9) to evaluate to next-to-leading order, as $\mu \to \infty$, the integrals $I_n(x)$ in the r.h.s. of Eq. (5.2). This procedure can then be repeated to obtain further corrections.

Eq. (5.9) provides the spherically symmetric, leading order singular solution of the mean field equation (2.13) where the particles are densely concentrated around one point in a region of size of the order of the cutoff A. In fact, to leading order in a the density reads

$$\rho(r) = \begin{cases} \frac{6}{\pi a^3}, & r \leqslant a/2, \\ 0, & r \geqslant a/2, \end{cases}$$

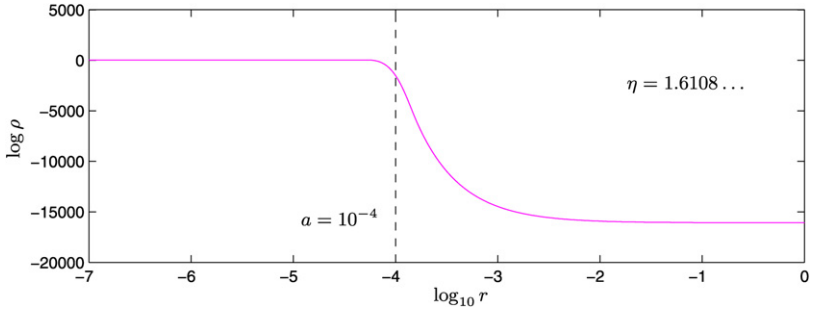

Fig. 6. Profiles of the logarithm of the density $\log\rho(r)$ for $\mu^2 = \mathcal{O}(\frac{1}{a})$ (collapsed solution). For the value of η given, we have $\lambda = 6012149.6972\ldots$. This collapsed profile should be compared to the dilute ones (stable and unstable) depicted in Fig. 2.

while to next-to-leading order we have

$$\rho(r) = \frac{6}{\pi a^3}\exp\left[\phi(r) - \frac{\eta}{a}\right], \tag{5.10}$$

where $\phi(r)$ has the leading order form of Eq. (5.9). This analytic behaviour agrees well with the numerical solution depicted in Fig. 6. This corresponds to the situation when the gravitational attraction completely overcomes the kinetic energy and all particles fall towards the origin. Of course, such singular solution only exist mathematically for non-zero values of the cutoff A.

Let us now compute the action for the solution Eq. (5.9) from Eq. (2.11). The regularized Laplacian can be computed from the equation of motion (2.13) with the leading order result for $a \to 0$,

$$\int\limits_{|\boldsymbol{r}|\leqslant 1} d^3r\,\phi(\boldsymbol{r})\nabla_a^2\phi(\boldsymbol{r}) = -\frac{4\pi\eta}{Q}4\pi\int\limits_0^1 r^2\,dr\,\phi(r)e^{\phi(r)} = -4\pi\eta\phi(0) = -\frac{4\pi\eta^2}{a}.$$

The second term is just

$$\log Q = \phi(0) - \log\frac{\lambda^2}{4\pi\eta} = \frac{\eta}{a} - \log\frac{6}{\pi a^3},$$

so that all together, to leading order we obtain for the free energy

$$\begin{aligned} F - F_0 = \frac{Gm^2\beta N}{2A} + NTs(\eta,a) &= \frac{Gm^2\beta N}{2A} - \frac{NT\eta}{2a} + NT\log\frac{8}{a^3} \\ &= -\frac{Gm^2N(N-1)}{2A} + NT\log\frac{R^3}{(A/2)^3}. \end{aligned} \tag{5.11}$$

The first term is just the potential energy of N particles clustered in a small sphere of radius $A/2$, where the regularized gravitational interaction is the same for all $\frac{1}{2}N(N-1)$ particle pairs. The second term is T times the entropy loss in the collapse. As one could expect, this free energy is large and negative, unbounded from below as $A \to 0$. In particular, this free energy is well below the free energy of the dilute solution Eq. (4.8) and Fig. 3 for all values $\eta > 0$. That is, the singular solution Eq. (5.9) provides the *absolute* minimum for the free energy Eq. (2.11) for any $\eta > 0$. The dilute solution Eqs. (4.4) and (4.2) is only a *local* minimum. In the next subsection we shall address the issue of the metastability of the dilute phase.

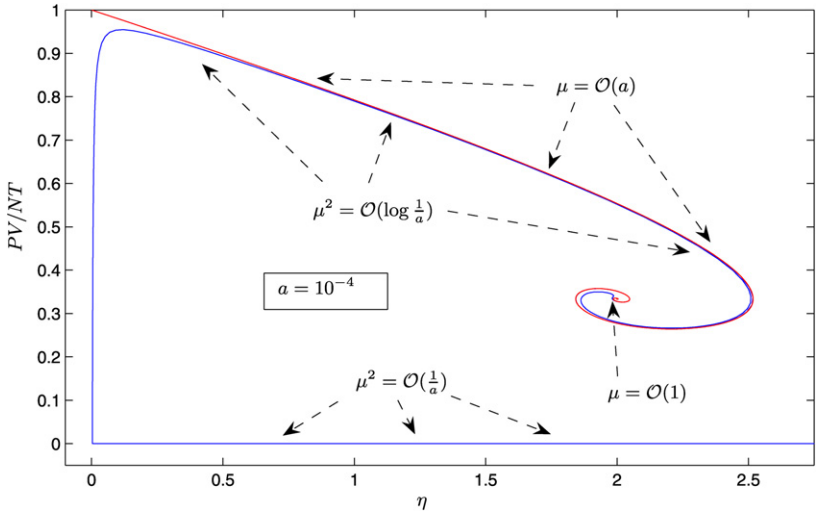

Fig. 7. Complete plot of PV/NT vs. η when $a = 10^{-4}$ (blue curve). When μ is of order a the blue curve cannot be distinguished from the corresponding curve of the case $a = 0$, here depicted in red (dilute solutions). When μ is of order 1 the blue curve ($a > 0$) and the red curve separate. The blue curve then traces the red spiral backwards at a distance of order $a(\log a)^2$ as long as $\mu^2 \lesssim \mathcal{O}(\log \frac{1}{a})$ (interpolating solutions). Finally the blue curve drops to zero when μ^2 is of order $\frac{1}{a}$ (collapsed solutions). (For interpretation of the references to colour in this figure legend, the reader is referred to the web version of this article.)

Let us now compute some physical quantities characterizing the collapsed phase.

The equation of state has the mean field form

$$\frac{PV}{NT} = \frac{4\pi}{3}\rho(1), \tag{5.12}$$

in both the dilute and collapsed phase. In the former case the r.h.s. of Eq. (5.12) coincides with the function $f(\eta)$. In the latter we obtain instead, from Eqs. (5.10) and (5.9), to next-to-leading order

$$\frac{PV}{NT} = \left(\frac{2}{a}\right)^3 \exp\left[\eta - \frac{\eta}{a}\right]. \tag{5.13}$$

Thus, the pressure at the boundary is exponentially small in the collapsed phase. The complete plot of PV/NT vs. η is given in Fig. 7. One can see how the well-known [3] spiraling towards $(\eta = 2, f(\eta) = 1/3)$, characteristic of the dilute solutions, is now limited to the case when μ is of order a. When μ reaches values of order 1 the inward spiral comes to a halt and then winds back until $\mu \lesssim \mathcal{O}(\log \frac{1}{a})$. For larger values of μ, that is $\mu \sim \eta/a$ as in the collapsed phase, PV/NT drops to values exponentially small in $\frac{1}{a}$. Analogous plots are obtained for other types of cutoff in Ref. [9].

For other physically relevant quantities we similarly find

$$c_V = \frac{3}{2}, \qquad c_P = \frac{3}{2} + \mathcal{O}(a^2), \qquad \frac{v_s^2}{T} = \frac{1}{\kappa_T} = \frac{8}{a^3}\exp\left[-\frac{\eta}{a}\right],$$
$$\frac{S - S_0}{N} = 3\log a + \mathcal{O}(a^0). \tag{5.14}$$

5.2. Interpolating solution: Metastability

The dilute solutions studied in Section 4 are metastable because the collapsed solution provides the absolute minimum for free energy [Eq. (5.11)]. The collapse transition from the dilute phase to the collapsed phase can take place through an interpolating solution in an analogous way to the bubbles in liquid–gas first order phase transitions [10].

Such interpolating solutions are the saddle points of Eq. (2.13), which correspond to the sudden drop of η as a function of $\log\lambda$ (see Fig. 4) located approximately at $\lambda^2 a^2 \sim \log\frac{1}{a}$. In this narrow drop region we have $\mathcal{O}(a) \lesssim \eta < \eta_C$, so the interpolating solutions are allowed only in this interval of η. Examples of the interpolating solutions are given in Fig. 5.

According to the qualitative discussion below Eq. (5.8), the location of the η drop can be obtained approximately as the values of λ at which the function $\chi(\lambda)$ has the crossover from the free solution $\chi(\lambda) \simeq c_0/\lambda + c_1$ to the logarithmic solution $\log(2/\lambda^2)$. That is for $\lambda^2 a^2 \sim \log\frac{1}{a}$, since $c_0 = \mathcal{O}(\lambda^3 a^3)$ and $c_1 = \mathcal{O}(\lambda^2 a^2)$, see Eq. (5.8). Then the scaling as $a \to 0$ of $\rho(0)$, the density in the origin, can be obtained from Eq. (5.1) and the numerical analysis as

$$\rho(0) = \frac{\lambda^2}{4\pi\eta} = \mathcal{O}\left(a^{-2}\log\frac{1}{a}\right),$$

because $\eta = \mathcal{O}(1)$ in this regime.

On the other hand, from Fig. 5 one sees that the value of the density for $r \gg a$ and in particular the value at the border $\rho(1)$ differ by order a w.r.t. the dilute phase. The equation of state (5.12), which holds for any value of λ, then implies that the pressure in the dilute and interpolating solution, for the same value of η, differ only by order a, as evident also from Fig. 7.

In practice, one can regard an interpolating configuration as a special spherical fluctuation of the dilute phase in which a fraction of particles of order $a\log\frac{1}{a}$ is almost uniformely removed from everywhere and concentrated in a region of size a around the origin. In fact, this result has an heuristic explanation by a simple energy-entropy argument: If we denote by $\Delta\rho$ the variation of the density in a region of size a around the origin, we then have

$$\Delta s \sim -\frac{\eta}{2a}\left(\frac{\Delta N}{N}\right)^2 + 3\frac{\Delta N}{N}\log\frac{1}{a}, \quad \frac{\Delta N}{N} \equiv a^3\Delta\rho, \tag{5.15}$$

since the first term is the gain in potential energy per particle and the second the loss of entropy per particle due to the concentration. We may neglect the effect due to the rest of the particles if we assume that $\frac{\Delta N}{N}$, the fraction of particle moved around, would vanish as $a \to 0$. Minimizing Eq. (5.15) w.r.t. $\Delta\rho$ yields

$$\Delta\rho \simeq \frac{3}{\eta a^2}\log\frac{1}{a} \quad \text{and} \quad \Delta s = \frac{9a}{2\eta}\left(\log\frac{1}{a}\right)^2, \tag{5.16}$$

which is indeed consistent with the requirement that $a^3\Delta\rho$ vanishes as $a \to 0$ and rather accurately approximate our numerical results.

Notice that the minimized Δs is to be identified with the difference, between interpolating and dilute solution, of the action per particle, so that

$$\Delta s = s_{\text{interpolating}} - s_{\text{dilute}} \simeq \frac{9}{2\eta}a(\log a)^2. \tag{5.17}$$

This result is in very good agreement with the numerical values obtained by solving Eqs. (3.3) and (3.6).

According to the interpretation of the interpolating solutions as saddle points through which the dilute phase may decay to the collapsed one, the lifetime of the dilute phase is given by

$$\tau \simeq \left(\frac{|\,\mathrm{Det}\,|}{\mathrm{Det}_0}\right)^{1/2} e^{N\Delta s}, \tag{5.18}$$

where Det stands for the determinant of small fluctuations around the interpolating solution and Det_0 for that around the dilute solution.

This ratio of determinants can be estimated as follows: In the interpolating profile there should be only one negative mode necessarily localized in a region of size a around the origin, where the density is very large, since $-\rho(r)$ plays the role of Schroedinger potential in the eigenvalue equation for the small fluctuations. Eq. (5.16) then implies that $\frac{1}{a^2}\log\frac{1}{a}$ provides the scale of the potential felt by this negative mode. Hence the corresponding negative eigenvalue should be of the same order, while the rest of the spectrum should be almost unaffected, since the two density profiles differ only by order a for $r \gtrsim 2a$. Therefore

$$\frac{|\,\mathrm{Det}\,|}{\mathrm{Det}_0} \simeq \frac{1}{a^2}\log\frac{1}{a}. \tag{5.19}$$

We obtain from Eqs. (5.17)–(5.19) to leading order the following lifetime for the dilute phase of the self-gravitating gas:

$$\tau \sim \frac{1}{a}\sqrt{\log\frac{1}{a}}\, e^{\frac{9N}{2\eta}a(\log a)^2} \sim \frac{R}{A}\sqrt{\log\frac{R}{A}}\exp\left[\frac{9AT}{2Gm^2}\left(\log\frac{R}{A}\right)^2\right]. \tag{5.20}$$

One can see that the lifetime becomes infinitely long in the zero cutoff limit as well as when $N \to \infty$ at fixed cutoff [recall that $R \sim N$ in the dilute limit of Eq. (1.1)].

We want to stress that the lifetime of the dilute solutions is extremely long for large N and small cutoff A. This is due to the fact that although the collapsed solution has a much lower energy than the dilute solution, in the latter there is a huge entropy barrier against the gathering, in a small domain of size $\sim A$, of a number particles large enough to start the collapse. A qualitatively similar conclusion is reached in Ref. [11].

We shall come back for a more detailed study of this problem in a subsequent paper.

References

[1] J. Binney, S. Tremaine, Galactic Dynamics, Princeton Univ. Press, Princeton, NJ, 1987;
P.J.E. Peebles, Principles of Physical Cosmology, Princeton Univ. Press, Princeton, NJ, 1993;
W.C. Saslaw, Gravitational Physics of Stellar and Galactic Systems, Cambridge Univ. Press, Cambridge, 1987.
[2] R.B. Larson, Mon. Not. R. Astron. Soc. 194 (1981) 809;
J.M. Scalo, in: D.J. Hollenbach, H.A. Thronson (Eds.), Interstellar Processes, Reidel, Dordrecht, 1987, p. 349.
[3] R. Emden, Gaskugeln, Teubner, Leipzig, 1907;
S. Chandrasekhar, An Introduction to the Study of Stellar Structure, Chicago Univ. Press, 1939;
R. Ebert, Z. Astrophys. 37 (1955) 217;
W.B. Bonnor, Mon. Not. R. Astron. Soc. 116 (1956) 351;
V.A. Antonov, Vest. Leningrad Univ. 7 (1962) 135;
D. Lynden-Bell, R. Wood, Mon. Not. R. Astron. Soc. 138 (1968) 495.
[4] E.B. Aronson, C.J. Hansen, Astrophys. J. 177 (1972) 145;
B. Stahl, M.K.H. Kiessling, K. Schindler, Planet Space Sci. 43 (1995) 271;
P. Hertel, W. Thirring, Commun. Math. Phys. 24 (1971) 22.
[5] H.J. de Vega, N. Sánchez, Nucl. Phys. B 625 (2002) 409, astro-ph/0101568.
[6] H.J. de Vega, N. Sánchez, Nucl. Phys. B 625 (2002) 460, astro-ph/0101567.

[7] H.J. de Vega, N. Sánchez, Statistical mechanics of the self-gravitating gas: Thermodynamic limit, phase diagrams and fractal structures, in: N. Sánchez, Yu. Parijskij (Eds.), Proceedings of the 9th Course of the International School of Astrophysics 'Daniel Chalonge', Palermo, Italy, 7–18 September 2002, NATO Adv. Sci. Inst., Kluwer, 2002, pp. 291–324, astro-ph/0505561.
[8] H.J. de Vega, J. Siebert, Phys. Rev. E 66 (2002) 016112;
H.J. de Vega, J. Siebert, Nucl. Phys. B 707 (2005) 529;
H.J. de Vega, J. Siebert, Nucl. Phys. B 726 (2005) 464;
H.J. de Vega, N. Sánchez, Nucl. Phys. B 711 (2005) 604.
[9] P.H. Chavanis, Phys. Rev. E 65 (2002) 056123;
P.H. Chavanis, I. Ispolatov, Phys. Rev. E 66 (2002) 036109;
P.H. Chavanis, J. Sommeria, Mon. Not. R. Astron. Soc. 296 (1998) 569;
E. Follana, V. Laliena, Phys. Rev. E 61 (2000) 6270.
[10] J.S. Langer, in: T. Riste (Ed.), Fluctuations, Instabilities and Phase Transitions, Plenum, New York, 1975, p. 19;
J.S. Langer, in: C. Godreche (Ed.), Solids Far From Equilibrium, Cambridge Univ. Press, 1992, p. 297;
L. Garrido, et al. (Eds.), Systems Far From Equilibrium, Lecture Notes in Physics, vol. 132, Springer, 1975;
J.D. Gunton, M. San Miguel, P.S. Sahni, in: C. Domb, J.J. Lebowitz (Eds.), Phase Transitions and Critical Phenomena, vol. 8, Academic Press, 1983;
J.S. Langer, Acta Metall. 21 (1973) 1649;
D. Boyanovsky, H.J. de Vega, D.J. Schwarz, Phase transitions in the early and the present Universe, hep-ph/0602002, Annu. Rev. Nucl. Part. Sci, in press.
[11] P.H. Chavanis, Astron. Astrophys. 432 (2005) 117.